



Design, modeling and control of a flying vehicle with a single moving part that can be positioned anywhere in space[☆]

Weixuan Zhang^{a,*}, Mark W. Mueller^b, Raffaello D'Andrea^a

^aInstitute for Dynamic Systems and Control, ETH Zurich, Sonneggstrasse 3, Zurich 8092, Switzerland

^bHigh Performance Robotics Lab, University of California, Berkeley, CA 94703, USA

ARTICLE INFO

Keywords:

Unmanned aerial vehicle
Highly underactuated flying vehicles
Controllability analysis of an unmanned aerial vehicle
Design of a highly underactuated flying vehicle
Control design of a highly underactuated flying vehicle

ABSTRACT

This paper presents a novel type of flying vehicle called the Monospinner, which has only one moving part, the propeller, and is yet able to hover and fully control its position. Its translational and attitude dynamics are formulated as a twelve-dimensional state space system, which may be linearized to a linear time-invariant system amenable to controllability analysis, controller synthesis, and vehicle design. It is shown that the linearized system may be both horizontally and vertically controllable in position after removing its yaw state, and in particular, this is shown for the case of a vehicle with the shape of a planar object and an offset thrust location (with respect to its center of mass). The vehicle's mass distribution is designed based on two robustness metrics: the ability to maintain hover under perturbations by means of Monte-Carlo nonlinear simulation, and the probability of input saturation based on a stochastic model. Experiments are conducted for the resulting vehicle and controller. The equilibrium of the resulting system has a large region of attraction such that it recovers after being thrown into the air like a frisbee.

1. Introduction

Highly underactuated flying vehicles have the advantages of increased reliability and reduced manufacturing and maintenance costs due to their reduced mechanical complexity. At the same time, this also leads to increased difficulty in the control of their attitude and position. Therefore, many researchers have explored the aerodynamic properties and the mass distributions of different vehicle designs that make the system's attitude passively stable ([1–10]): if the vehicle in hover is disturbed and tilts away or moves sideways, aerodynamic forces will damp out the lateral motion and induce a restoring moment, bringing the vehicle's attitude back to its hover state and its translational velocity to zero. The vehicle's position will not recover to its position before the disturbance, which means that its position is not passively stable. While eliminating the need for attitude sensing (onboard sensors such as gyroscope, attitude estimation, etc.) and active attitude control, this can limit the vehicle's maneuverability, as its actuators have to counteract these restoring aerodynamic forces and moments to achieve controlled forward flight.

This paper presents a different approach: a highly underactuated vehicle (called the “Monospinner” and shown in Fig. 1¹) is designed with-

out relying on aerodynamic effects (apart from the airframe drag torque and the propeller) or attitude passive stability. It has a single moving part (its rotating propeller), and its attitude is stabilized by active feedback control. While attitude sensing is required for the Monospinner, active attitude control increases the vehicle's maneuverability. The vehicle is fully controllable in position. To the best of the authors' knowledge, there exist only two types of vehicles (the other one is the Maneuverable Piccolissimo [8]) that are both horizontally and vertically controllable with only one moving part.

This article includes a formulation of the Monospinner's translational and attitude dynamics in a twelve dimensional state space and its corresponding equilibrium. With the linearized system matrices at hand, the system is analyzed as a whole and its controllability leads to a definitive answer to whether the vehicle is controllable in position. It is shown that the full twelve state system is not stabilizable for any vehicle configuration. However, the system may be fully controllable in position after removing the yaw state, as it does not affect the dynamics of other states. This reduced eleven state system is thus investigated. Specifically, three types of vehicle configuration under simplifying assumptions are analyzed, giving guidelines for the mechanical design of the vehicle. A linear, time-invariant controller is designed to control the hovering

[☆] This paper was recommended for publication by Associate Editor Prof. Dr. Lei Zuo.

* Corresponding author.

E-mail addresses: wzhang@ethz.ch (W. Zhang), mwm@berkeley.edu (M.W. Mueller), rdandrea@ethz.ch (R. D'Andrea).

¹ A video showing the Monospinner can be found under <https://youtu.be/P3fM6VwXXFM>.

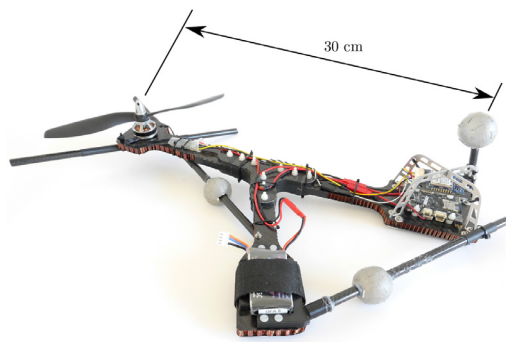


Fig. 1. The Monospinner is approximately 30 cm in size, the frame consists of five carbon-fiber plates, and the electronics are mounted in an aluminium cage. The carbon fiber rods help to protect the propeller during landing. A more detailed list of components is given in [Table 1](#).

vehicle, and a vehicle design is found by optimizing mainly for the vehicle's mass distribution. Two robustness metrics are chosen: the ability to maintain hover under perturbations and the probability of input saturation based on a stochastic model. Experimental results showed that the resulting vehicle is not only able to hover, but also has a large region of attraction such that it recovers after being thrown into the air like a frisbee.

1.1. Related work

A vehicle similar to the Monospinner is the Maneuverable Piccolissimo: it also features only one moving part (the propeller) and one actuator and is yet fully controllable in position. While aiming for small size (the vehicle is 39 mm in its largest dimension and 4.47 g in weight), the authors designed the vehicle's mass distribution and relative rotor speed to achieve passive stability in attitude. With an offset between its thrust location and the center of mass, the whole body rotates in the air with a small tilt angle. Horizontal control is achieved by modulating its thrust at a rate of once per body revolution and thus creating net moments and forces that control its roll, pitch and position.

Highly-underactuated flying machines can be categorized into several subgroups: The first category is the samara-type vehicle, which can be traced back to the 1950's [11] and is also referred to as the Monocopter. Inspired by the maple seed (or samara), the vehicle's whole body is similar to that of a samara or a single wing and rotates around the vertical axis during flight. Rotation is usually achieved by the thrust produced by a propeller mounted at one end of the body, and the lift created by this rotation counterbalances the vehicle's weight. Through proper vehicle design, Monocopters become passively stable in attitude [12] and can hover for a trimmed open loop control input. With a servo-driven control surface installed on the wing, they may be controllable in the horizontal plane. Thus, they require two actuators to be fully controllable in position. Notable references are [2–7], which focused on aspects related to the modeling, design, and control of the Monocopters. A more detailed study and modeling on the Monocopter's system dynamics, especially regarding its aerodynamic properties, can be found in [13,14].

Vehicles in the second category are equipped with one actuator (a rotating propeller), providing thrust in the vertical direction and inducing body rotation around the vertical axis, while aerodynamic dampers are installed to make sure that they are passively stable in attitude. The thrust produced goes through the center of mass and can only control the height of the vehicle. Such vehicles are presented in [1,8], while similar vehicles exist as toys, for example the Air Hogs Vectron [15] or Flower Flutterby Fairy [16].

The third category is the flapping-wing flying vehicle. Biologically inspired, their main propulsion comes from the flapping of a pair of

wings, and aerodynamic dampers are often installed to ensure passive attitude stability. In [9,10], the presented flying vehicles have one actuator and are only controllable in height. In [17–19], the flying vehicles have at least two actuators to achieve controlled forward flight.

Traditional small scale helicopters are not passively stable in attitude and require servo-controlled swashplates for attitude control, which results in at least three actuators. In [20], the authors presented a coaxial helicopter that uses only two actuators to control the vehicle's roll, pitch, and yaw orientation, as well as maneuvering thrust. For roll and pitch control, one actuator uses a pair of passively hinged airfoil blades to mimic a conventional helicopter's cyclic control and generate torque around the roll and pitch axes. The other actuator is equipped with a conventional fixed-pitch propeller, and thrust and yaw control are achieved by the collective thrust and the differential propeller reaction torque of these two actuators. In [1], the author presented a prototype called the UNO that uses the same passive hinge mechanism to achieve horizontal, roll, and pitch control. It has one actuator (the motor) and three moving parts (the passively hinged propeller).

Another category is the flying vehicle with no moving parts. These are actuated by an ionic jet engine, which produces thrust by emitting positively charged ions and harvesting momentum from their collisions with a neutral fluid. In [21], a robotic airfish with an ionic jet and plasma ray propulsion system is presented. However, there is little information about its capabilities. In [22], the flying vehicle presented has a similar configuration to a standard quadcopter and uses four ion thrusters (thus four actuators) instead of four propeller-based thrusters. Simulation shows controlled flight, and the vehicle prototype is able to have an open-loop, uncontrolled takeoff. Another class of vehicles with arguably no moving parts are spacecraft operating only under thrusters (e.g. lunar landers) – they typically have significant redundancy, with substantially more actuators than degrees of freedom, and thus do not fit into the category of underactuated vehicles considered in this work.

Vehicles in the last category have only fixed-pitch propellers with parallel axes of rotation as inputs, and they are fully controllable in position. In [23,24] it is shown that a quadcopter can maintain flight despite the complete loss of two propellers (that is, with only two propellers remaining) and in theory, control is possible after the complete loss of three propellers. The Monospinner (one propeller), the Bispinner (two propellers) [24], and the Maneuverable Piccolissimo belong to this category. The Monospinner and the Bispinner require active attitude control, whereas the Maneuverable Piccolissimo does not, since it is passively stable in attitude.

In [23], the authors derived conditions under which two degrees of freedom in attitude are controllable for three different propeller loss cases (that is, complete loss of one, two or three propellers) for a quadcopter. They also derived in [24] a general framework for establishing attitude controllability of the vehicles in the last category and investigated a special case where a quadcopter loses two opposing motors. In [25], a controllability test method is developed for multicopter systems with positive thrust constraints and around their conventional hover state (zero translational and rotational velocity).

This paper follows previous work presented at a conference [26] and extends these previous results by presenting:

- a twelve-dimensional state-space system description for the Monospinner, for which an equilibrium exists and where techniques from linear time-invariant system theory may be applied for system analysis and control design,
- a proof that the twelve-dimensional linearized system about hover is not stabilizable for any vehicle configuration,
- controllability analysis of the reduced eleven-dimensional linearized system (with yaw state removed) for three special types of vehicle configuration,
- the experimental results with a controller designed using the proposed linear system model, which enables the resulting vehicle to move anywhere in space.

The remainder of this paper is organized as follows: the dynamic model of the Monospinner is given in Section 2, together with a twelve-state system description and its equilibrium solution. A linearized system is obtained and a controllability analysis is given in Section 3. A linear controller for the system is derived in Section 4, and the vehicle design based on two robustness metrics is discussed in Section 5. The resulting vehicle is presented in Section 6. Experimental results including two types of takeoff are shown in Section 7, followed by a conclusion given in Section 8.

2. Modeling and dynamics

This section provides the dynamic model for analysis and control of the Monospinner, followed by the discussion of the hover equilibrium of the resulting twelve-state system.

2.1. Dynamic model

This model is the same as the one given in [26] and summarized here for the sake of completeness. Fig. 2 shows some of the salient forces and quantities used in this section. The vehicle has a total mass m , and the gravity vector is denoted as \mathbf{g} . Boldface symbols like \mathbf{g} are used throughout the paper to denote vectors in three-dimensional space. The propeller produces a thrust force of magnitude f_p in the direction of the unit vector \mathbf{n}_p . The position of the vehicle's center of mass with respect to a point fixed in the inertial frame is denoted as \mathbf{s} .

Two coordinate systems are used for the modeling: an inertial (ground-fixed) coordinate system E and a body-fixed coordinate system B . A vector expressed in a specific coordinate system is indicated by a superscript, for example \mathbf{g}^E expresses \mathbf{g} in coordinate system E . The body-fixed coordinate system B is oriented such that the motor arm (Fig. 2) is parallel with its x -axis and the propeller axis of rotation is aligned with its z -axis. The propeller force vector \mathbf{n}_p^B is then $(0,0,1)$. The notation $(0,0,1)$ is used throughout this paper to compactly express the elements of a column vector.

The translational dynamics of the vehicle, expressed in the inertial frame E , are captured by Newton's law:

$$\ddot{\mathbf{s}}^E = m^{-1} \mathbf{n}_p^E f_p + \mathbf{g}^E \quad (1)$$

where it is assumed that the vehicle travels at low translational velocities, such that translational drag forces (such as those described in [27]) are neglected.

Let I_p denote the moment of inertia of the propeller (referred to the spin axis), and let $I_B + I_p$ denote the total moment of inertia of the vehicle (with respect to its center of mass). The vehicle rotates at an angular

velocity ω_{BE} with respect to the coordinate system E , where the subscript BE means the relative velocity of coordinate system B with respect to E . The propeller is located at a displacement \mathbf{r}_p with respect to the center of mass, and its angular velocity with respect to the coordinate system E is denoted as ω_{pE} . Besides the thrust f_p , the propeller also experiences a torque of magnitude τ_p in the propeller thrust direction \mathbf{n}_p due to the aerodynamic drag acting on the propeller blade, which is transmitted to the body through the motor. The vehicle experiences an airframe drag torque τ_d due to the rotation of the vehicle in the air.

The angular dynamics of the system, expressed in the body-fixed coordinate system B , are formulated as:

$$I_B^B \dot{\omega}_{BE}^B + I_p^B \dot{\omega}_{pE}^B + [\omega_{BE}^B \times] (I_B^B \omega_{BE}^B + I_p^B \omega_{pE}^B) = [[r_p^B \times] \mathbf{n}_p^B f_p + \mathbf{n}_p^B \tau_p + \tau_d^B \quad (2)$$

where $[\mathbf{a} \times]$ represents the skew-symmetric matrix form of the cross product, so that $[\mathbf{a} \times] \mathbf{b} = \mathbf{a} \times \mathbf{b}$ for any vectors \mathbf{a} and \mathbf{b} in \mathbb{R}^3 .

Without loss of generality, it is assumed that the propeller is left-handed. The propeller's scalar speed Ω with respect to the body is usually controlled by an electronic speed controller, so that

$$\omega_{pB}^B = (0, 0, -\Omega). \quad (3)$$

Note that ω_{pE}^B in (2) can be decomposed as below:

$$\omega_{pE}^B = \omega_{pB}^B + \omega_{BE}^B. \quad (4)$$

The thrust f_p produced from a stationary propeller is then assumed to be proportional to its angular velocity ω_{pE}^B squared with the proportional coefficient κ_f [28]:

$$f_p = \kappa_f (\omega_{pE}^B \cdot \mathbf{n}_p^B) |\omega_{pE}^B \cdot \mathbf{n}_p^B| \quad (5)$$

with \cdot denoting the vector inner product.

The propeller torque is assumed to be linear in the propeller thrust:

$$\tau_p = \kappa f_p \quad (6)$$

We neglect any potential torque effects due to blade flapping [29] or the propeller H-force [27].

It is assumed that the magnitude of the airframe drag torque τ_d is quadratic in the vehicle's angular velocity ω_{BE}^B [24]:

$$\tau_d^B = -\|\omega_{BE}^B\| \mathbf{K}_d^B \omega_{BE}^B \quad (7)$$

where $\|\cdot\|$ denotes the Euclidean norm and \mathbf{K}_d is a 3×3 matrix and assumed to be diagonal when expressed in the coordinate system B , which is denoted by

$$\mathbf{K}_d^B = \text{diag}(K_{d,xx}, K_{d,yy}, K_{d,zz}). \quad (8)$$

It is assumed that the different propeller speeds near the operating point discussed in the paper are not significant enough to make a difference in the drag torque that the vehicle experiences. Therefore it is assumed that the propeller's contribution to the drag torque is constant and implicitly included in (7).

2.2. Hover solution

Similar to Section 2.1, the Monospinner's hover solution is derived in [26] and summarized here for the sake of completeness. This hover solution follows the definition of the "relaxed hover solutions" [24], which are defined as solutions that are constant when expressed in a body-fixed reference frame and where the vehicle remains substantially in one position. Specifically, these solutions allow the vehicle to have a non-zero translational acceleration (but it must average to zero) and a non-zero angular velocity.

In hover, the Monospinner's center of mass has a uniform circular motion and stays at a constant height, while the vehicle body is rotating at a constant angular velocity ω_{BE}^B in the parallel direction of gravity. Note that the overbar in this paper is always used to denote quantities

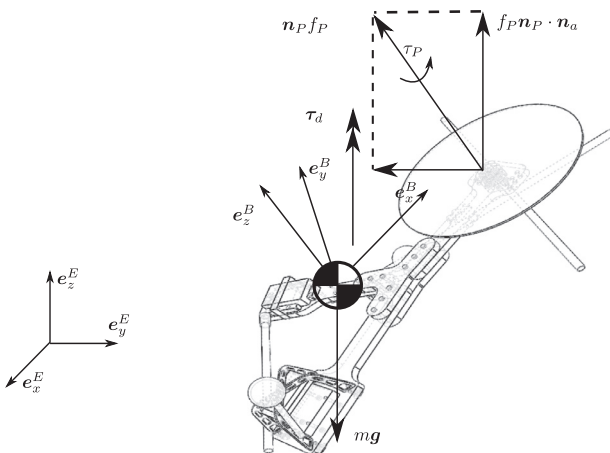


Fig. 2. Monospinner in flight, showing some of the symbols and quantities required to model the system.

that are constant in hover (i.e. the equilibrium solution). Also, a body-fixed unit vector \mathbf{n}_a exists, which does not change when expressed in the coordinate system E . This vector may be thought of as an averaged thrust direction of the vehicle: in hover it is aligned with the thrust vector averaged over one rotation. Note that the instantaneous thrust direction may not be aligned with gravity.

Furthermore, the vector \mathbf{n}_a is parallel to $\bar{\omega}_{BE}$:

$$\mathbf{n}_a^B = \frac{\bar{\omega}_{BE}^B}{\bar{\omega}}, \quad (9)$$

where $\bar{\omega}$ is the magnitude of the equilibrium angular velocity $\|\bar{\omega}_{BE}^B\|$.

The equilibrium propeller force $\mathbf{n}_p^B \bar{f}_p$ can be decomposed into horizontal and vertical forces, where the horizontal force induces the circular motion and the vertical force compensates for the vehicle's weight. Thus

$$\bar{f}_p \mathbf{n}_p^B \cdot \mathbf{n}_a^B = m \|\mathbf{g}\|. \quad (10)$$

Substituting (9) into (10) yields the following solution for the equilibrium thrust

$$\bar{f}_p = \frac{m \|\mathbf{g}\| \bar{\omega}}{\mathbf{n}_p^B \cdot \bar{\omega}_{BE}^B}. \quad (11)$$

In hover (i.e. setting the derivatives to zero), (2) becomes:

$$\llbracket \bar{\omega}_{BE}^B \times \rrbracket (\mathbf{I}_B^B \bar{\omega}_{BE}^B + \mathbf{I}_p^B \bar{\omega}_{pE}^B) = \llbracket \mathbf{r}_p^B \times \rrbracket \mathbf{n}_p^B \bar{f}_p + \mathbf{n}_p^B \bar{\tau}_p + \bar{\tau}_d^B. \quad (12)$$

Note that the quantities $\bar{\omega}_{pE}^B$, \bar{f}_p , $\bar{\tau}_p$ and $\bar{\tau}_d^B$ are uniquely defined by $\bar{\Omega}$ and $\bar{\omega}_{BE}^B$ (see (3)–(7)), such that we have four equations in four unknowns. The hover solution is therefore defined by the $\bar{\Omega}$ and $\bar{\omega}_{BE}^B$ that solve (11) and (12). With the resulting $\bar{\Omega}$ and $\bar{\omega}_{BE}^B$ (if they exist) all other quantities in hover (such as \mathbf{n}_a^B or \bar{f}_p) may be calculated.

2.3. Equilibrium

In this section two frames (see Fig. 3) are introduced: a body frame convenient for the controllability analysis and control design, and a rotating reference frame for obtaining attitude equilibrium. Translational and attitude equilibrium is solved using the hover solution in Section 2.2.

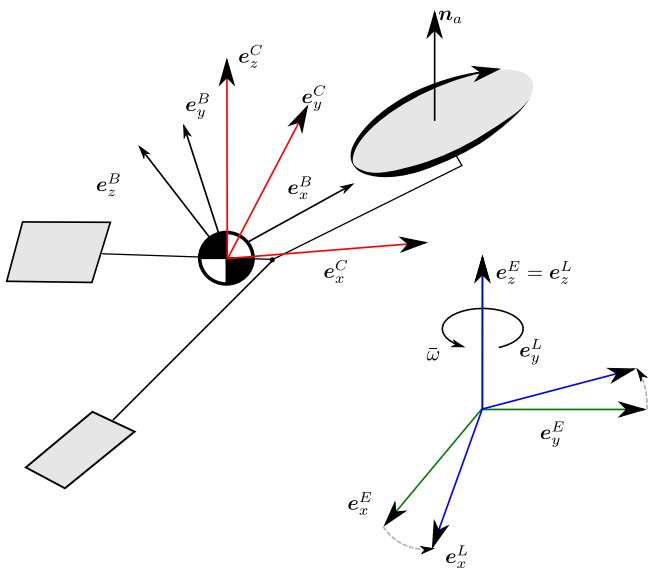


Fig. 3. This figure illustrates the two frames introduced in Section 2.3: the body-fixed C -frame is introduced such that the body-fixed unit vector \mathbf{n}_a is aligned with its z -axis, and the propeller force vector \mathbf{n}_p^C has no y -component. The L -frame rotates at a constant angular speed $\bar{\omega}$ around the gravity vector and therefore the z -axis of the inertial frame E .

2.3.1. Attitude equilibrium

For convenience, a body-fixed C -frame is introduced such that

$$\mathbf{n}_a^C = \mathbf{R}^{CB} \mathbf{n}_a^B = (0, 0, 1) \quad (13)$$

Note that (13) remains valid if the C -frame rotates around its z -axis. This degree of freedom may be fixed by the constraint that the propeller thrust direction \mathbf{n}_p^C has no y component when expressed in the C -frame, that is,

$$\mathbf{n}_p^C = \mathbf{R}^{CB} \mathbf{n}_p^B \stackrel{!}{=} (*, 0, *) \quad (14)$$

Let $(p, q, r) := \omega_{CE}^C$ be the body rates expressed in the C -frame. By (9) and (13) the body rates equilibrium $\bar{\omega}_{CE}^C$ is

$$\bar{\omega}_{CE}^C = \bar{\omega}_{BE}^C = \mathbf{R}^{CB} \bar{\omega}_{BE}^B = \mathbf{R}^{CB} \mathbf{n}_a^B \bar{\omega} = (0, 0, \bar{\omega}). \quad (15)$$

In other words, at equilibrium the body-fixed C -frame is rotating at a constant angular speed $\bar{\omega}$ about the gravity vector and the yaw angle between the C and the E -frame increases linearly with time. In order to have a constant yaw equilibrium, a frame L rotating at a constant angular speed $\bar{\omega}$ around the gravity vector is introduced with

$$\omega_{LE}^L = (0, 0, \bar{\omega}). \quad (16)$$

Then the vehicle's orientation may be represented by \mathbf{R}^{CL} , which relates the body-fixed frame C and the frame L . We parametrize the rotation matrix \mathbf{R}^{CL} through the Euler Yaw-Pitch-Roll sequence, following the common aerospace convention [30], with ϕ (roll), θ (pitch), and ψ (yaw):

$$\mathbf{R}^{CL} = \mathbf{R}_x(\phi) \mathbf{R}_y(\theta) \mathbf{R}_z(\psi) \quad (17)$$

where

$$\mathbf{R}_x(\phi) = \begin{bmatrix} 1 & 0 & 0 \\ 0 & \cos \phi & \sin \phi \\ 0 & -\sin \phi & \cos \phi \end{bmatrix} \quad (18)$$

$$\mathbf{R}_y(\theta) = \begin{bmatrix} \cos \theta & 0 & -\sin \theta \\ 0 & 1 & 0 \\ \sin \theta & 0 & \cos \theta \end{bmatrix} \quad (19)$$

$$\mathbf{R}_z(\psi) = \begin{bmatrix} \cos \psi & \sin \psi & 0 \\ -\sin \psi & \cos \psi & 0 \\ 0 & 0 & 1 \end{bmatrix}. \quad (20)$$

In hover, it is clear from (15) and (16) that there is only a constant yaw offset (the equilibrium yaw angle) between the C -frame and the L -frame. Therefore, the equilibrium pitch and roll angles are both zero, that is, $\bar{\theta} = \bar{\phi} = 0$. Note that the equilibrium yaw angle ($\bar{\psi}$) depends only on the choice of the initial yaw between the L and E -frame and is therefore set to zero without loss of generality. The rotation matrix \mathbf{R}^{CL} may alternatively be parametrized with a 3-1-3 Euler angle sequence, consisting of spin, nutation, and precession [31]. This parametrization is popular for describing spinning bodies, but is less useful than the proposed yaw-pitch-roll sequence as it has a singularity at the equilibrium with zero nutation angle.

2.3.2. Translational equilibrium

Since in hover the center of mass of the vehicle is rotating in a circle at a constant height, its horizontal position and velocity are oscillatory when expressed in the inertial frame. Thus, the position and velocity states are expressed in the body frame C , and their dynamics are obtained by applying Euler's transformation on the position vector \mathbf{s} and velocity vector \mathbf{v} :

$$\dot{\mathbf{s}}^C = \mathbf{v}^C - \llbracket \omega_{CE}^C \times \rrbracket \mathbf{s}^C \quad (21)$$

$$\dot{\mathbf{v}}^C = \mathbf{R}^{CE}(\dot{\mathbf{s}})^E - \llbracket \omega_{CE}^C \times \rrbracket \mathbf{v}^C \quad (22)$$

$$= \frac{1}{m} \mathbf{n}_p^C \bar{f}_p + \mathbf{R}^{CE} \mathbf{g}^E - \llbracket \omega_{CE}^C \times \rrbracket \mathbf{v}^C \quad (23)$$

where $\mathbf{v} := \dot{\mathbf{s}}$ and (1) is substituted into (22).

Setting (23)'s left hand side to zero and substituting the hover solution into the equation yields

$$0 = \frac{1}{m} n_p^C \bar{f}_p + \bar{\mathbf{R}}^{CE} \mathbf{g}^E - \llbracket \bar{\omega}_{CE}^C \times \rrbracket \bar{\mathbf{v}}^C. \quad (24)$$

Recall that in hover the C-frame rotates about the gravity vector, thus $\bar{\mathbf{R}}^{CE} \mathbf{g}^E = \mathbf{g}^E$. Substituting the body rates equilibrium solution (15) and solving (24) yields

$$\bar{v}_y^C = -\frac{\bar{f}_p n_{p,x}^C}{\bar{\omega} m}, \quad \bar{v}_x^C = \frac{\bar{f}_p n_{p,y}^C}{\bar{\omega} m} = 0, \quad (25)$$

where $(n_{p,x}^C, n_{p,y}^C, n_{p,z}^C) := \mathbf{n}_p^C$, $(\bar{v}_x^C, \bar{v}_y^C, \bar{v}_z^C) := \bar{\mathbf{v}}^C$. The equilibrium state $\bar{\mathbf{v}}^C$ is equal to 0 since $n_{p,y}^C$ is zero according to (14).

Setting the left hand side of (21) to zero, substituting the hover solution into it, and solving the equation yields:

$$\bar{v}_z^C = 0, \quad \bar{s}_y^C = -\frac{\bar{v}_x^C}{\bar{\omega}} = 0, \quad \bar{s}_x^C = \frac{\bar{v}_y^C}{\bar{\omega}} = -\frac{\bar{f}_p n_{p,x}^C}{\bar{\omega}^2 m}, \quad (26)$$

where $(\bar{s}_x^C, \bar{s}_y^C, \bar{s}_z^C) := \bar{\mathbf{s}}^C$.

Note that \bar{s}_z^C does not appear in the equilibrium equations and is set to zero without loss of generality. The fact that the horizontal position equilibrium \bar{s}_x^C and \bar{s}_y^C cannot be set arbitrarily is simply a feature of choice of the state and the coordinate system it is represented in.

2.3.3. Equilibrium solution

In conclusion, the twelve-state equilibrium $(\bar{s}_x^C, \bar{s}_y^C, \bar{s}_z^C, \bar{v}_x^C, \bar{v}_y^C, \bar{v}_z^C, \bar{\phi}, \bar{\theta}, \bar{\psi}, \bar{p}, \bar{q}, \bar{r})$ is:

$$\begin{aligned} \bar{s}_x^C &= -\frac{\bar{f}_p n_{p,x}^C}{\bar{\omega}^2 m}, \quad \bar{s}_y^C = 0, \quad \bar{s}_z^C = 0 \\ \bar{v}_x^C &= 0, \quad \bar{v}_y^C = -\frac{\bar{f}_p n_{p,x}^C}{\bar{\omega} m}, \quad \bar{v}_z^C = 0, \\ \bar{\phi} &= 0, \quad \bar{\theta} = 0, \quad \bar{\psi} = 0, \\ \bar{p} &= 0, \quad \bar{q} = 0, \quad \bar{r} = \bar{\omega}. \end{aligned} \quad (27)$$

3. Linearized system and controllability analysis

In this section, the attitude kinematics for the Euler angles (ϕ, θ, ψ) that were introduced earlier are derived. The resulting twelve-state dynamic system is linearized about hover and the controllability analysis is subsequently given.

3.1. Linearization

The angular rates ω_{CL}^C and the rates of the Euler angles $(\dot{\phi}, \dot{\theta}, \dot{\psi})$ have the following relationship [30]:

$$\omega_{CL}^C = \begin{bmatrix} \dot{\phi} \\ 0 \\ 0 \end{bmatrix} + \mathbf{R}_x(\phi) \begin{bmatrix} 0 \\ \dot{\theta} \\ 0 \end{bmatrix} + \mathbf{R}_x(\phi) \mathbf{R}_y(\theta) \begin{bmatrix} 0 \\ 0 \\ \dot{\psi} \end{bmatrix}, \quad (28)$$

the inverse mapping of which (that is, the mapping from ω_{CL}^C to $(\dot{\phi}, \dot{\theta}, \dot{\psi})$) has the following form:

$$\begin{bmatrix} \dot{\phi} \\ \dot{\theta} \\ \dot{\psi} \end{bmatrix} = \begin{bmatrix} 1 & \sin(\phi) \tan(\theta) & \cos(\phi) \tan(\theta) \\ 0 & \cos(\phi) & -\sin(\phi) \\ 0 & \sin(\phi)/\cos(\theta) & \cos(\phi)/\cos(\theta) \end{bmatrix} \omega_{CL}^C \quad (29)$$

Note that

$$\omega_{CL}^C = \omega_{CE}^C - \omega_{LE}^C = \omega_{CE}^C - \mathbf{R}^{CL} \omega_{LE}^L \quad (30)$$

Substituting (30) into (29) yields

$$\begin{bmatrix} \dot{\phi} \\ \dot{\theta} \\ \dot{\psi} \end{bmatrix} = \begin{bmatrix} 1 & \sin(\phi) \tan(\theta) & \cos(\phi) \tan(\theta) \\ 0 & \cos(\phi) & -\sin(\phi) \\ 0 & \sin(\phi)/\cos(\theta) & \cos(\phi)/\cos(\theta) \end{bmatrix} \left(\omega_{CE}^C + \begin{bmatrix} \sin(\theta) \bar{\omega} \\ -\sin(\phi) \cos(\theta) \bar{\omega} \\ -\cos(\theta) \cos(\phi) \bar{\omega} \end{bmatrix} \right) \quad (31)$$

Introducing the state deviation from the equilibrium defined in (27)

$$x = (\delta s_x^C, \delta s_y^C, \delta s_z^C, \delta v_x^C, \delta v_y^C, \delta v_z^C, \delta \phi, \delta \theta, \delta \psi, \delta p, \delta q, \delta r), \quad (32)$$

defining the control input u as deviation of the motor force from the equilibrium motor force \bar{f}_p , and linearizing the system dynamics (21), (23), (31) and (2) about the equilibrium yield a linear, time-invariant (LTI) system:

$$\dot{x} \approx Ax + Bu. \quad (33)$$

Substituting the equilibrium solution $\bar{\phi} = \bar{\theta} = 0$ into (33) ($\bar{\psi}$ does not appear in the linearization), the system matrices A and B become

$$A = \begin{bmatrix} -\llbracket \bar{\omega}_{CE}^C \times \rrbracket & I_3 & 0 & \llbracket \bar{s}^C \times \rrbracket \\ 0 & -\llbracket \bar{\omega}_{CE}^C \times \rrbracket & -\llbracket \mathbf{g}^E \times \rrbracket & \llbracket \bar{v}^C \times \rrbracket \\ 0 & 0 & -\llbracket \bar{\omega}_{CE}^C \times \rrbracket & I_3 \\ 0 & 0 & 0 & A_S^C \end{bmatrix}, \quad B = \begin{bmatrix} 0 \\ m^{-1} \mathbf{n}_p^C \\ 0 \\ B_S^C \end{bmatrix}. \quad (34)$$

Every entry of A in the above expression denotes a 3 by 3 matrix and every entry of B denotes a 3 by 1 matrix. A_S^C and B_S^C denote the linearization matrices of the Euler's Eq. (2), and I_3 is an identity matrix of dimension 3. Note that the appearance of \bar{s}_z^C in the system matrix A comes from the fact that the position state is formulated in the body frame. It does not, however, affect the controllability of the system pair (see Section 3.2.2, \bar{s}_z^C does not appear in the matrices in (37)–(39)).

3.2. Controllability analysis

In this section, controllability analysis for the linearized system is conducted to gain intuition of when it is possible to control the Monospinner. It will be shown that the full twelve-state system (from now on referred to as the full state system) is never stabilizable², and the controllability test of the reduced eleven state system (with yaw state removed and from now on referred to as the reduced state system) is equivalent to the full rank tests of at most five matrices (two 4×4 matrices and three 3×4 matrices). The controllability analysis of three special cases for the reduced state system is subsequently given.

3.2.1. The full state system

Note that the matrix A in (34) is an upper block diagonal matrix. The spectrum of A is therefore the union of the spectra of the diagonal block matrices, that is,

$$\text{spec}(A) = \text{spec}(\llbracket \bar{\omega}_{CE}^C \times \rrbracket) \cup \text{spec}(A_S^C) \quad (35)$$

The spectrum of the skew-symmetric matrix $\llbracket \bar{\omega}_{CE}^C \times \rrbracket$ is $\{0, \pm i, -\bar{\omega}i, 0\}$, with i denoting the imaginary unit. The eigenvalues of A are then divided into three categories: 0, $\pm i$ and the eigenvalues of A_S^C .

For a linear, time-invariant system, one could apply the Popov–Belevitch–Hautus (PBH) test to investigate its controllability (Corollary 12.6.19, [33]), the pair (A, B) is controllable if and only if for all eigenvalues λ of A , the concatenated matrix $[\lambda I - A \ B] \in \mathbb{C}^{12 \times 13}$ has full rank. This includes the case of eigenvalue 0, where the test matrix has the form $[-A \ B]$. Note that the third and the ninth column of the matrix A are zero vectors, meaning that the concatenated test matrix $[-A \ B]$ has at most rank 11 and therefore does not have full rank. The pair (A, B) is thus not stabilizable. Note that including the translational drag forces (such as those described in [27]) in (23) would not change the system's stabilizability, as they do not depend on the yaw and height of the vehicle and thus this does not change the rank of the test matrix $[-A \ B]$.

² In this article, controllability of an LTI system is defined to mean that for any initial state, there exists a control trajectory such that the system can be steered from that state to 0 in finite time, whereas stabilizability is defined to mean that for any initial state, there exists a control trajectory such that the system state converges to zero as time goes to infinity [32].

3.2.2. The reduced state system and equivalent controllability tests

Rearranging the states in (32) (moving the yaw state $\delta\psi$ to the last state) yields:

$$\tilde{A} = \begin{bmatrix} A_{11} & 0 \\ A_{21} & 0 \end{bmatrix}, \quad \tilde{B} = \begin{bmatrix} B_1 \\ 0 \end{bmatrix} \quad (36)$$

with $A_{11} \in \mathbb{R}^{11 \times 11}$, $A_{21} \in \mathbb{R}^{1 \times 11}$, $B_1 \in \mathbb{R}^{11 \times 1}$ and 0 being the zero matrix with associated dimension. From (36), it can be seen that the yaw state does not affect the dynamics of other states.

Furthermore, changing the yaw state (the yaw angle between the L and the C -frame) in hover would not affect the direction of the averaged thrust, and therefore not the roll angle, pitch angle, and position in the inertial frame. This motivates investigating the controllability of the system without the yaw state, that is, the system matrix pair (A_{11}, B_1) . Stabilizability of this reduced state system implies the ability of the system to maintain a relaxed hover solution while rejecting disturbances (e.g. a step change in reference position), remaining substantially at one point in space (though the yaw angle may not be able to simultaneously achieve some setpoint). Note that the stabilizability of the reduced system also implies that the yaw rate of the vehicle stays bounded.

The PBH test is then applied to the reduced system matrix pair (A_{11}, B_1) . Applying the algebra outlined in Appendix A, it is revealed that for the eigenvalue 0, the matrix $[-A_{11} \ B_1]$ has full rank if and only if the matrix $U_0 \in \mathbb{R}^{4 \times 4}$ has full rank, where

$$U_0 = \begin{bmatrix} V_0 & -(A_S^C)^\top \\ m^{-1}n_{P,z}^C & (B_S^C)^\top \end{bmatrix} \quad (37)$$

with $V_0 = (\bar{v}_y^C, 0, 0)$.

Similarly, for the eigenvalues $\pm\omega i$, since $[\omega i I - A_{11} \ B_1]$ and $[-\omega i I - A_{11} \ B_1]$ have the same rank (Fact 2.19.3, [33]), it suffices to investigate $[\omega i I - A_{11} \ B_1]$, which has full rank if and only if the matrix $U_i \in \mathbb{C}^{4 \times 4}$ has full rank (Appendix A), where

$$U_i = \begin{bmatrix} V_i & \omega i I - (A_S^C)^\top \\ 0 & (B_S^C)^\top \end{bmatrix} \quad (38)$$

with $V_i = (1, -i, 0)$.

Finally, for the eigenvalues of A_S^C , assuming that its eigenvalues are distinct from 0 and $\pm\omega i$ (otherwise we can check the rank of U_0 or U_i), its associated full rank tests are equivalent to the test of whether or not the matrix $U_s(\lambda) : \mathbb{C} \mapsto \mathbb{C}^{3 \times 4}$ has full rank (Appendix A), where

$$U_s(\lambda) = [\lambda I - A_S^C \quad B_S^C] \quad (39)$$

with $\lambda \in \text{spec}(A_S^C)$.

In summary, the system pair (A_{11}, B_1) is stabilizable if and only if U_0, U_i have full rank, and $U_s(\lambda)$ has full rank for the eigenvalues of A_S^C whose real part is non-negative. Also note that obtaining the matrices A_S^C and B_S^C symbolically is nontrivial, since it requires the knowledge of the equilibrium solution to define the C -frame, and solving the nonlinear Eqs. (11) and (12) symbolically for the equilibrium is in most cases very tedious, if not impossible.

3.2.3. Special cases for the reduced state system

In this section, special cases under simplifying assumptions are investigated to provide intuition of when the reduced state system matrix pair (A_{11}, B_1) is stabilizable. This may be useful since if the system is stabilizable for the simplified system equations, then it will be stabilizable for the actual system, provided that the modeling error is small enough. This stems from the fact that the eigenvalues of a matrix are continuous functions of its elements (Fact 10.11.9, [33]) that are also locally continuous at the model parameters. Therefore, the PBH test matrix does not lose rank for a perturbation of the system matrices that is small enough. Conversely, if the system is not stabilizable for the simplified system equations, it may still be stabilizable for the actual system, but it is very likely that large control efforts would be required to stabilize it.

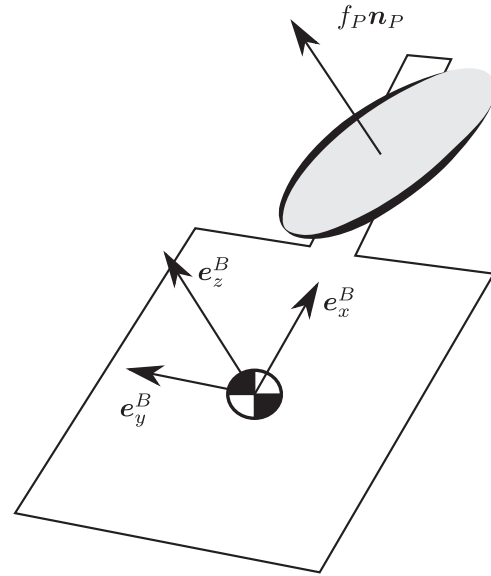


Fig. 4. A possible shape of the vehicle in the special case 1 of the controllability analysis for the reduced state system. It is a planar object with an offset thrust location.

First, it is assumed that the terms $I_P^B \dot{\omega}_{PE}^B$ and $I_P^B \omega_{PE}^B$ are negligible. For a typical vehicle design (that is, the vehicle is roughly the size of a quadcopter described in [34]), the largest component of the propeller moment of inertia I_P^B (the moment of inertia around its body z -axis) is two orders of magnitude smaller than the smallest diagonal entries of the vehicle moment of inertia I_B^B , and the equilibrium angular momentum term $I_P^B \dot{\omega}_{PE}^B$ is an order of magnitude smaller than $I_B^B \dot{\omega}_{BE}^B$. The Euler's Eq. (2) thus becomes

$$I_B^B \dot{\omega}_{BE}^B + [\omega_{BE}^B \times] I_B^B \omega_{BE}^B = [r_P^B \times] n_P f_P + n_P^B \tau_P + \tau_d^B. \quad (40)$$

It is also assumed that the vehicle's angular velocity with respect to the inertial frame is much smaller than the propeller's angular velocity with respect to the body, i.e., $\|\omega_{BE}\| \ll \|\omega_{PB}\|$, so that f_P is not a function of the body rates.

The following three special cases are then investigated:

Case 1

It is first assumed that the vehicle is a planar object (Fig. 4). The perpendicular axis theorem applies then, that is, for a coordinate system where the object is lying in the xy -plane, the sum of the moments of inertia about axis x and y is equal to the moment of inertia about axis z . Furthermore, the vehicle's inertia matrix is assumed to be diagonal in the B -frame. In summary, $I_B^B = \text{diag}(\Theta_x, \Theta_y, \Theta_x + \Theta_y)$.

It is assumed that the propeller thrust location has a positive offset to the center of mass, that is, $r_P^B = (l, 0, 0)$, with l being positive. It is also assumed that the vehicle's equilibrium pitch and roll rates are small, such that the airframe drag torque around the body x and y -axes is neglected:

$$\tau_d^B = (0, 0, -K r_B |r_B|), \quad (41)$$

where K is a positive constant and r_B is the yaw rate in the B -frame. In a typical vehicle design, it is found that the terms $[\omega_{BE}^B \times] I_B^B \dot{\omega}_{BE}^B$ and $[r_P^B \times] n_P f_P$ are at least an order of magnitude larger than the airframe drag torque around the body x and y -axes. A further reason for this assumption is that, intuitively, for such a fast, almost flat wobbling planar object, the gyroscopic effect and the offset propeller thrust dominate the roll and pitch rate dynamics, whereas the propeller torque has to be counterbalanced by the airframe drag torque in the body z -axis.

It is shown that in this case the reduced system matrix pair (A_{11}, B_1) is always stabilizable (see B.1). This implies that a vehicle of flat shape is a viable choice when designing a Monospinner. A special

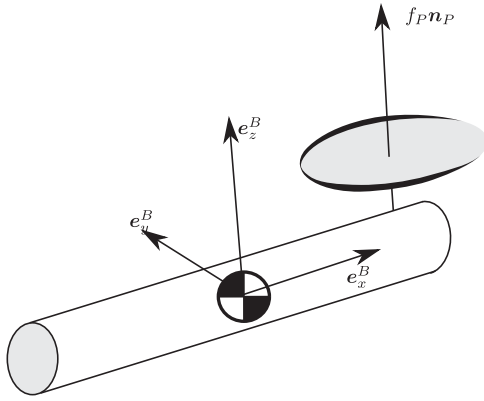


Fig. 5. A possible shape of the vehicle in the special case 2 of the controllability analysis for the reduced state system. It has the shape of a cylinder and the thrust location goes through the cylinder's center axis.

case here is when the vehicle has the shape of a flat plate, that is, $I_B^B = \text{diag}(\Theta, \Theta, 2\Theta)$. The Maneuverable Piccolissimo [8], for instance, has such an inertia distribution.

Case 2

It is assumed that the vehicle's inertia matrix has the form $I_B^B = \text{diag}(\Phi, \Theta, \Theta)$, and the airframe drag matrix expressed in the body frame B has the form $K_d^B = \text{diag}(J, K, K)$, where Φ, Θ, J , and K are non-zero. Here the vehicle's equilibrium pitch and roll rates may not be small, thus the aerodynamic effects in the pitch and roll axes cannot be neglected. As in case 1, it is assumed that the thrust location r_p^B is equal to $(l, 0, 0)$ with positive l . This corresponds to the case where the vehicle has the shape of a cylinder and the thrust location is aligned with its center axis (Fig. 5). Note that this case also includes the special case that the vehicle's mass distribution is symmetric, that is, $I_B^B = \text{diag}(\Theta, \Theta, \Theta)$ (e.g. a sphere or cube).

It can be proved that the reduced state system is *not stabilizable*, since the PBH test matrix associated with the eigenvalues on the imaginary axis does not have full rank (see B.2). Intuitively, the cross-coupling term (the term $[\omega_{BE}^B \times] J_B^B \omega_{BE}^B$ in the Euler's equation) in the x -axis disappears due to the structure of the inertia matrix, so that the roll rate dynamics can be hardly influenced by other states. In addition, the propeller thrust only creates moment around the pitch axis. The reduced state system is therefore not stabilizable. This indicates that when designing a Monospinner, the design should avoid to have an inertia matrix similar to the one given in this case.

Case 3

In this case, the propeller thrust location r_p is assumed to be equal to $(0, 0, 0)$. Assume the vehicle's inertia matrix has the form $I_B^B = \text{diag}(\Theta_x, \Theta_y, \Theta_z)$. Then one equilibrium of this special case is $\bar{p}_B = 0, \bar{q}_B = 0, \bar{r}_B = \sqrt{\kappa \bar{f}_P / K_{d,zz}}$, where $(\bar{p}_B, \bar{q}_B, \bar{r}_B) := \bar{\omega}_{BE}^B$. It can be shown that the linearized reduced state system around this equilibrium is uncontrollable (B.3).

This is also intuitively easy to see, namely, due to the lack of the cross-coupling term in hover and the term $[\mathbf{r}_p^B \times] \mathbf{n}_p^B f_P$ in the x and y -axis, the control input could influence the yaw rate dynamics, but not the roll and pitch rate dynamics. This indicates that when designing a Monospinner, the thrust location should not be too close to the center of mass.

4. Control strategy

The above analysis indicates that by giving up the control of yaw, the reduced state system may be stabilized by a state feedback controller. Recall that the vehicle's position can still be controlled.

Furthermore, the motor dynamics may have a large influence on the system, if the time constant of their response to commands is comparable to the time constants of the remainder of the system. For this reason the motor force is also included as a state, and is approximated by a first order system with time constant τ_{mot} :

$$\dot{f}_P = \tau_{\text{mot}}^{-1}(f_{\text{com}} - f_P) \quad (42)$$

where f_{com} is the command thrust for the propeller and f_P is the current propeller thrust.

Augmenting the deviation of the motor force from the equilibrium force (i.e. $f_P - \bar{f}_P$) as a state to the reduced state system, denoting the new state as x , and introducing the new control input $u := f_{\text{com}} - \bar{f}_P$, the augmented state system equation is then

$$\dot{x} \approx A_c x + B_c u \quad (43)$$

Note that although the motor force state (or equivalently, the motor speed) represents a degree of freedom of the system, including it in the state space or not does not affect the system's controllability, as the motor force is considered directly as the input to the system in the latter case. From now on, it is always assumed that the system matrix pair (A_c, B_c) is controllable, such that a stabilizing feedback controller may be designed.

An infinite-horizon linear-quadratic regulator (LQR) [35] may be readily designed with the cost on the position states set to $1\text{m}^{-2}\text{s}^{-1}$, cost on the roll and pitch states set to $10\text{m}^{-2}\text{s}^{-1}$, cost on the input set to $1\text{m}^{-2}\text{s}^{-1}$, and cost on the rest of the states set to 0, yielding a static feedback gain K :

$$u = -Kx. \quad (44)$$

The resulting thrust command is then:

$$f_{\text{com}} = \bar{f}_P + u. \quad (45)$$

Note that the controller presented here is different from the one in the conference version [26]: it is a single linear controller that regulates both translational and attitude states, whereas the controller in the conference version employs a cascaded control scheme that exploits time scale separation. This full state control strategy may bring advantages if the desired position dynamics have a similar time constant to the desired attitude dynamics. It also allows for the investigation of the stability margin of the closed-loop system and addressing the issue of actuator saturation, by designing a model predictive controller that takes the input constraint into account while considering the position at the same time.

5. Design

Since the system has only limited control authority at its disposal, it is important to find the vehicle design that is least sensitive to uncertainties such as parametric uncertainties and measurement noise. This section presents the methods to find a vehicle configuration such that the vehicle is sufficiently robust against these uncertainties.

5.1. Simplified mechanical model

To allow for efficient evaluation, a simplified mechanical model is used for the analysis, where there are three major components in the vehicle: the battery, the electronics and the motor (including the propeller). The components' contribution to the composite inertia matrix is approximated as follows: the three major components are approximated as point masses and the connecting frame components are approximated as thin rods. From the inertia matrix (and by assuming that the vehicle has similar drag coefficients as the quadcopter in [34]), the resulting vehicle's equilibrium solution and the linearized system matrices can be computed as described in the preceding sections.

By measuring the weights of the available components of the prototype, the battery is taken to have a weight of 0.06 kg, the electronics 0.045 kg and the motor 0.04 kg. The connecting rods are taken to have a length density of 0.06kg m^{-1} .

5.2. Choosing the vehicle configuration

The vehicle design focuses on optimizing over the vehicle's mass distribution. One motivation here is that a mass distribution where the cross-coupling term (i.e. the gyroscopic effect) dominates in hover would make the system's body rate dynamics more coupled and therefore easier to control.

The vehicle's approximate size and shape are based on the existing trispinner [24], with a Y-shape and a vehicle diameter of approximately 30 cm. The positions of the battery and the motor are fixed to be two vertices of an equilateral triangle, while the position of the electronics is to be determined.

A two-dimensional grid search of the position of the electronics is then conducted, where two different quality metrics are considered. The first is the probability of input saturation and is based on the linear, time-invariant model of the dynamic system. The second metric uses Monte Carlo simulations of the nonlinear system, including parameter perturbations and noise, to approximate the probability that the resulting vehicle is able to maintain hover. The probability of input saturation may be computed in closed form for a given design and is therefore cheap to evaluate, but is less informative than the Monte Carlo simulations.

5.2.1. Probability of input saturation

In feedback control, system noise may be amplified into the control input command and cause input saturation even if the system is near equilibrium. It is therefore important to know how measurement and process noise relates to the actual input force, specifically how likely it leads to input saturation. This is particularly true for the Monospinner: with the available motor and propeller, the hover propeller force is near saturation (about 75% of the maximum available thrust). In the following, a stochastic analysis is presented: a discretized version of the linear system is derived and augmented with measurement and actuator noise, which is identified by dedicated experiments. The probability that input saturation occurs may then be computed in closed-form.

Discretizing the system (43) with a zero-order-hold on the input $u[k]$ leads to:

$$x[k + 1] = A_d x[k] + B_d u[k] \quad (46)$$

where A_d and B_d are the discretized system matrices.

The measurement outputs are taken to be those available on the experimental platform, that is, every state except the linear velocity. The measurement $z[k]$ is then

$$z[k] = C_d x[k] + w_{\text{meas}}[k] \quad (47)$$

where $w_{\text{meas}}[k] \in \mathbb{R}^9$ is the measurement noise, which is assumed to be zero-mean, white, and Gaussian. Furthermore, $C_d \in \mathbb{R}^{9 \times 12}$ has the form

$$C_d = \begin{bmatrix} I_3 & 0 & 0 \\ 0 & 0 & I_6 \end{bmatrix} \quad (48)$$

where I_3 and I_6 are identity matrices with dimension 3 and 6, and 0 is the zero matrix with associated dimension. Clearly, the system matrix pair (A_d, C_d) is observable.

With \hat{x} defined as the state estimate, a steady-state Kalman filter has the following form:

$$\hat{x}[k] = (I_{12} - K_f C_d)(A_d \hat{x}[k - 1] + B_d u[k - 1]) + K_f z[k] \quad (49)$$

where K_f is the filter gain and I_{12} is the identity matrix with dimension 12.

The controller input follows from applying the discrete LQR gain K_d . It is also assumed that white, Gaussian, and zero-mean actuator noise $w_{\text{act}}[k]$ exist and act on the system. The true control input $u_{\text{true}}[k]$ is then

$$u_{\text{true}}[k] = -K_d \hat{x}[k] + w_{\text{act}}[k]. \quad (50)$$

Introducing the extended state $\tilde{x}[k] = (x[k], \hat{x}[k])$ and noise $\tilde{w}[k] = (w_{\text{meas}}[k + 1], w_{\text{act}}[k])$, substituting (50) into (46) yields

$$x[k + 1] = A_d x[k] - B_d K_d \hat{x}[k] + B_d w_{\text{act}}[k] \quad (51)$$

Substituting (51) into (47) and then into (49) leads to

$$\begin{aligned} \hat{x}[k] = & K_f C_d A_d x[k - 1] + ((I_{12} - K_f C_d) A_d - B_d K_d) \hat{x}[k - 1] \\ & + B_d w_{\text{act}}[k - 1] + K_f w_{\text{meas}}[k] \end{aligned} \quad (52)$$

Combining (50)–(52) and introducing the corresponding extended system matrices \tilde{A} , \tilde{B} , \tilde{C} and \tilde{D} , the extended system equations are:

$$\tilde{x}[k + 1] = \tilde{A} \tilde{x}[k] + \tilde{B} \tilde{w}[k] \quad (53a)$$

$$u_{\text{true}}[k] = \tilde{C} \tilde{x}[k] + \tilde{D} \tilde{w}[k]. \quad (53b)$$

By separation theorem for LTI systems and quadratic cost [35], the extended system (53a) is stable with a stable feedback controller and a stable state estimator. Thus, the extended system will reach steady state (the equilibrium) as k goes to infinity. Let $P_{\tilde{w}}$, $P_{\tilde{x}}$ and $P_{u_{\text{true}}}$ be the variables' associated steady-state covariance matrices (e.g. $P_{\tilde{x}} = \text{Var}(\tilde{x}[k])$ for $k \rightarrow \infty$). Through the steady state equations of (53a) and (53b), the covariance matrices have the following relationship:

$$P_{\tilde{x}} = \tilde{A} P_{\tilde{x}} \tilde{A}^T + \tilde{B} P_{\tilde{w}} \tilde{B}^T \quad (54a)$$

$$P_{u_{\text{true}}} = \tilde{C} P_{\tilde{x}} \tilde{C}^T + \tilde{D} P_{\tilde{w}} \tilde{D}^T. \quad (54b)$$

Note that (54a) is a discrete-time Lyapunov equation, for which a solution $P_{\tilde{x}}$ is guaranteed to exist, since \tilde{A} is discrete-time asymptotically stable, and $\tilde{B} P_{\tilde{w}} \tilde{B}^T$ is positive semi-definite (Proposition 11.10.6 [33]). Furthermore, since the measurement noise variance $P_{\tilde{w}}$ is measured from experiment, and \tilde{A} and \tilde{B} are known, $P_{\tilde{x}}$ can be readily solved by (54a). Substituting the solution into (54b) gives the variance of the actuator $P_{u_{\text{true}}}$.

Since the noise $\tilde{w}[k]$ is assumed to be Gaussian and zero-mean, $u_{\text{true}}[k]$ is also Gaussian and zero-mean at steady state. As a result, the propeller thrust at equilibrium is a Gaussian random variable with mean \bar{f}_p and variance $P_{u_{\text{true}}}$, from which the probability of saturating the maximal allowed thrust may be calculated. Note that this allows for capturing the fact that a design with low variance may still have a high probability of saturation if it has a high mean thrust. In this way the saturation probabilities of varying positions of the electronics are computed and shown in Fig. 6, and the results are discussed in the following.

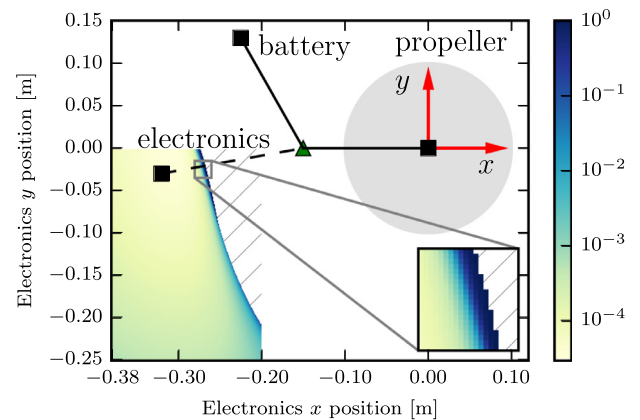


Fig. 6. The probability of the input saturation for one time step for varying positions of the electronics. In the colored area, a grid search with resolution 0.001 m both in x and y -direction is conducted. Electronics positions for which a hover solution cannot be solved are marked with hatching (the upper right corner of the color area). Note that the color bar has logarithmic scale. Note that on the boundary between the regions that has equilibrium solutions and that has no solution, there is a rapid increase of the input saturation probabilities. This is due to the rapid increase in the equilibrium motor force at this boundary. The chosen position of the electronics is also plotted.

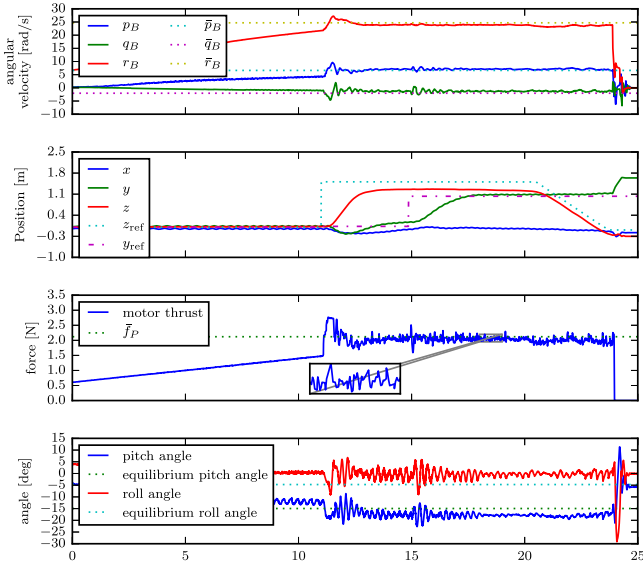


Fig. 8. Experimental results for the Monospinner's take-off from the platform. The vehicle takes off at 11 s and lands at 20 s. At time 15 s, a reference position change of 1 m is set in the (horizontal) y -direction. Note that at steady-state there is an offset between the vehicle's height z and the reference height z_{ref} . This is due to the discrepancy between the expected hover solution and the true hover solution and it may be readily compensated by adding an integral term to the position control. The angular velocity is plotted as expressed in the body-fixed coordinate system, where $\omega_{BE}^B = (p_B, q_B, r_B)$. The roll and pitch angles are the standard Euler sequence (1,2,3) angles from the E -frame to the B -frame. The attached video shows such an experiment.

7.1. Take-off from a platform

Ideally, one would like the Monospinner to start near the equilibrium, especially in terms of its body rates: if instead the equilibrium thrust is applied when the vehicle has zero angular velocity (e.g. it is at rest on the ground), the vehicle would simply flip over. This is because the cross-coupling term (i.e. the gyroscopic effect) and the airframe drag torque are second-order terms in the angular velocity and thus negligible. Moreover, the propeller's pitch torque is larger than its yaw torque due to the vehicle's geometry: the torque to thrust ratio of the propeller is of the order of 1.5 cm, and the propeller thrust moment arm is 15 cm. Thus, a passive mechanism is designed to allow the Monospinner achieve an angular velocity close to its equilibrium before taking off. The mechanism consists of a platform, on which the Monospinner rests, connected by a bearing to the ground, so that the vehicle can freely rotate about its vector \mathbf{n}_a . The rotation is achieved solely through the propeller torque τ_p , and the thrust is slowly ramped up from zero to the equilibrium solution. Once sufficiently close to equilibrium, the full control is switched on and the vehicle takes off. A representative state history during a take-off is shown in Fig. 8. The equilibrium body rates of the vehicle in hover are as below, which may be compared to the expected values in (60) and (61)

$$\bar{\omega}_{BE} = (6.9, -1.2, 24.8) \text{ rad s}^{-1} \quad (62)$$

$$\bar{f}_P = 2.12 \text{ N}. \quad (63)$$

7.2. Hand launch

Alternatively, the Monospinner can be launched by throwing it like a frisbee. This is a faster method of achieving hover than the takeoff mechanism in Section 7.1, and shows that the resulting system's equilibrium has a large region of attraction. A representative state history during a hand-launch is shown in Fig. 9.

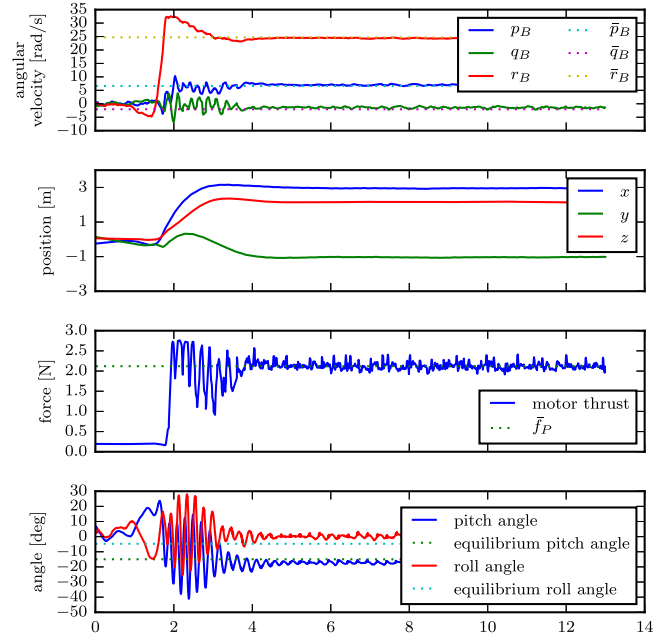


Fig. 9. Experimental results for a successful hand launch of the Monospinner. Its initial angular velocity has about 30% deviation of the equilibrium angular velocity, and its initial roll and pitch both have about 20° deviation of the equilibrium roll and pitch. The vehicle is thrown at approximately 2 s, after which the controller is switched on. The angular velocity is plotted as expressed in the body-fixed coordinate system, where $\omega_{BE}^B = (p_B, q_B, r_B)$. The roll and pitch angles are the standard Euler sequence (1,2,3) angles from the E -frame to the B -frame. The attached video shows such an experiment.

8. Conclusion

This paper presents the modeling, design, and control of a flying vehicle with only one moving part and a single control input, which is able to fully control its position and may be used as novel hobbyist platforms, toys, or low-cost flying vehicles. First, the vehicle's coupled translational and attitude dynamics are formulated as a twelve state system for which an equilibrium exists. This allows for analysis of the linearized system using the powerful tools from linear system theory. Then a controllability analysis is given: It is shown that the full state system is never stabilizable, and after removing the yaw state, the reduced state system maybe fully controllable in position. In particular, the reduced state system is always stabilizable for a class of vehicles that has the shape of a planar object and an offset thrust location with respect to the center of mass. The resulting vehicle may be approximated by an instance of this class of vehicles and its corresponding system matrix pair is shown to be indeed stabilizable. An LQR controller for the reduced state system is designed and is shown to work reliably in the experiments. A vehicle design method is also presented: it optimizes mainly over the vehicle's shape and hence its mass distribution, in order to find a design that is robust against system noise and parametric uncertainties. Finally, the resulting vehicle is shown to be capable of hovering and its equilibrium has a large region of attraction such that the vehicle recovers to hover after being thrown into the air like a frisbee. An area of additional investigation may be the analysis of the presented linear controller and the determination of the region of attraction of the resulting equilibrium.

Declaration of Competing Interest

The authors declare that they have no known competing financial interests or personal relationships that could have appeared to influence the work reported in this paper.

Acknowledgments

This research was partially supported by the SNF Grant 162365. The authors would like to thank Michael Egli, Marc-Andr  Corzillius and Yilun Wu for their contribution to the mechanical design, electrical design and the onboard firmware code, respectively. The authors would also like to thank Michael Muehlebach for critically reading a draft of this manuscript and for valuable discussions. The Flying Machine Arena is the result of contributions of many people, a full list of which can be found at <http://flyingmachinearena.org/>.

Appendix A. Equivalent controllability tests for the reduced state system

In this appendix it will be shown that the matrices $[-A_{11} \ B_1]$, $[\pm\bar{\omega}iI - A_{11} \ B_1]$ and $[\lambda I - A_{11} \ B_1]$ with $\lambda \in \text{spec}(A_S^C)$ have full rank if and only if the matrices U_0 (37), U_i (38), and $U_s(\lambda)$ (39) have full rank, respectively.

According to [36], the system matrix pair (A_{11}, B_1) is uncontrollable if and only if there exists a $v \neq 0$ with

$$v^T A_{11} = \lambda v^T, \quad v^T B_1 = 0, \tag{A.1}$$

where λ and its associated left eigenvector v is an uncontrollable mode. Therefore, to determine whether the test matrix $[\lambda I - A_{11} \ B_1]$ has full rank is equivalent to solving for a non-zero solution v in the equation $v^T[\lambda I - A_{11} \ B_1] = 0$ (e.g. if there exists a non-zero v , then the test matrix does not have full rank, and vice versa). In the following, the equation will be solved for each eigenvalue of A_{11} , which are 0, $\pm\bar{\omega}i$, and the eigenvalues of the submatrix A_S^C .

Eigenvalue $\lambda = 0$

Taking the transpose of the matrices on both sides of the equation yields

$$[-A_{11} \ B_1]^T v = 0. \tag{A.2}$$

Denote $v \in \mathbb{R}^{11}$ by $v = [v_1, v_2, v_3, v_4]$ with $v_1, v_2, v_4 \in \mathbb{R}^3$ and $v_3 = (v_{31}, v_{32}) \in \mathbb{R}^2$. In total, there are 12 equations.

Solving the first three equations of (A.2),

$$-[\bar{\omega}_{CE}^C \times] v_1 = 0, \tag{A.3}$$

leads to $v_1 = \alpha \bar{\omega}_{CE}^C$, where $\alpha \in \mathbb{R}$.

The next three equations are

$$-v_1 - [\bar{\omega}_{CE}^C \times] v_2 = 0. \tag{A.4}$$

Substituting $v_1 = \alpha \bar{\omega}_{CE}^C$ into (A.4) yields $\alpha = 0$ and thus $v_1 = 0$, and $v_2 = \beta \bar{\omega}_{CE}^C$, with $\beta \in \mathbb{R}$.

From the 7th and the 8th equations it follows that

$$\begin{bmatrix} 0 & \bar{\omega} \\ -\bar{\omega} & 0 \end{bmatrix} \begin{bmatrix} v_{31} \\ v_{32} \end{bmatrix} = 0, \tag{A.5}$$

yielding $v_3 = 0$.

The last four equations are

$$[\bar{v}^C \times] v_2 - (A_S^C)^T v_4 = 0 \tag{A.6}$$

and

$$m^{-1}(\bar{n}_p^C)^T v_2 + (B_S^C)^T v_4 = 0. \tag{A.7}$$

Its solution depends on the entries of A_S^C and B_S^C , which are functions of the vehicle's physical parameters.

In summary, the existence of the solution of (A.2) is equivalent to the existence of the solution of the following equation:

$$\underbrace{\begin{bmatrix} V_0 & -(A_S^C)^T \\ m^{-1} \bar{n}_{p,z}^C & (B_S^C)^T \end{bmatrix}}_{=: U_0} \begin{bmatrix} v_{23} \\ v_4 \end{bmatrix} = 0 \tag{A.8}$$

with $V_0 = (\bar{v}_y^C, 0, 0)$ and v_{23} denoting the third component of v_2 . Thus there exists a non-zero solution for (A.2) if and only if the matrix U_0 does not have full rank.

Eigenvalue $\lambda = \pm\bar{\omega}i$

As pointed out in Section 3.2.2, only the case of $\lambda = \bar{\omega}i$ needs to be investigated. The equation to be solved is

$$[i\bar{\omega}I - A_{11} \ B_1]^T v = 0. \tag{A.9}$$

Solving the first three equations

$$(i\bar{\omega}I - [\bar{\omega}_{CE}^C \times]) v_1 = 0. \tag{A.10}$$

This leads to $v_1 = (\alpha, -i\alpha, 0)$, with $\alpha \in \mathbb{R}$.

The next three equations are

$$(i\bar{\omega}I - [\bar{\omega}_{CE}^C \times]) v_2 - v_1 = 0. \tag{A.11}$$

It follows that $\alpha = 0$ and thus $v_1 = 0$, and $v_2 = (\beta, -i\beta, 0)$, with $\beta \in \mathbb{R}$.

From the 7th to the 8th equations

$$\begin{bmatrix} 0 & \|\mathbf{g}\| \\ -\|\mathbf{g}\| & 0 \end{bmatrix} \begin{bmatrix} \beta \\ -i\beta \end{bmatrix} + \begin{bmatrix} i & 1 \\ -1 & i \end{bmatrix} \bar{\omega} v_3 = 0. \tag{A.12}$$

The result follows as $\beta = 0$, which leads to $v_2 = 0$, and $v_3 = (\gamma, -i\gamma)$.

The last four equations are

$$\begin{bmatrix} 1 & 0 \\ 0 & 1 \\ 0 & 0 \end{bmatrix} \begin{bmatrix} \gamma \\ -i\gamma \end{bmatrix} + (i\bar{\omega}I_3 - A_S^C)^T v_4 = 0 \tag{A.13}$$

$$(B_S^C)^T v_4 = 0, \tag{A.14}$$

the solution of which depends on the parameters of A_S^C and B_S^C .

In summary, the existence of a non-zero solution for (A.9) is equivalent to the existence of a non-zero solution for the following equation

$$\underbrace{\begin{bmatrix} V_i & \bar{\omega}iI - (A_S^C)^T \\ 0 & (B_S^C)^T \end{bmatrix}}_{U_i} \begin{bmatrix} \gamma \\ v_4 \end{bmatrix} = 0 \tag{A.15}$$

where $V_i = (1, -i, 0)$. This is the case if and only if the matrix U_i does not have full rank.

Eigenvalues of A_S^C

Recall that it is assumed that the eigenvalues of A_S^C are distinct from 0 and $\pm\bar{\omega}i$ (otherwise we can check the rank of U_0 or U_i). Therefore, the upper left 9 by 9 block matrix of $[\lambda I - A_{11} \ B_1]$ has full rank, and it suffices to investigate the rank of its lower right 3 by 4 block matrix $[\lambda I - A_S^C \ B_S^C]$ (Fact 2.11.13 [33]).

Appendix B. Controllability analysis for three special cases of the reduced state system

In Section 3.2.3, controllability analysis is performed for three special cases of reduced state system under simplifying assumptions. In this appendix, details of derivation are shown for each case.

B1. Controllability analysis for case 1

In this case (for assumptions see Section 3.2.3), we will show that the system is at least stabilizable. Let $\omega_{BE}^B = (p_B, q_B, r_B)$. Writing out the simplified Euler's Eq. (40) under the proposed assumptions for case 1 yields

$$\dot{p}_B = -q_B r_B \tag{B.1}$$

$$\dot{q}_B = p_B r_B - \frac{1}{\Theta_y} f_P \tag{B.2}$$

$$\dot{r}_B = \frac{\Theta_x - \Theta_y}{\Theta_x + \Theta_y} p_B q_B - \frac{K}{\Theta_x + \Theta_y} r_B^2 + \frac{\kappa}{\Theta_x + \Theta_y} f_P. \tag{B.3}$$

Setting the right hand side of the above three equations to zero yields three nonlinear equations, from which the equilibrium body rates $(\bar{p}_B, \bar{q}_B, \bar{r}_B)$ may be solved:

$$0 = \bar{q}_B \bar{r}_B \tag{B.4}$$

$$0 = \bar{p}_B \bar{r}_B - \frac{1}{\Theta_y} \bar{f}_P \tag{B.5}$$

$$0 = \frac{\Theta_x - \Theta_y}{\Theta_x + \Theta_y} \bar{p}_B \bar{q}_B - \frac{K}{\Theta_x + \Theta_y} \bar{r}_B^2 + \frac{\kappa}{\Theta_x + \Theta_y} \bar{f}_P. \tag{B.6}$$

Solving the above equations yields:

$$\bar{p}_B = \frac{1}{\Theta_y} \sqrt{\frac{\bar{f}_P}{\kappa}}, \quad \bar{q}_B = 0, \quad \bar{r}_B = \sqrt{\kappa \bar{f}_P}. \tag{B.7}$$

Linearizing (B.1)–(B.3) around $(\bar{p}_B, \bar{q}_B, \bar{r}_B)$ and \bar{f}_P yields

$$A_S^B = \begin{bmatrix} 0 & -\bar{r}_B & 0 \\ \bar{r}_B & 0 & \bar{p}_B \\ 0 & D\bar{p}_B & -2k\bar{r}_B \end{bmatrix}, \quad B_S^B = \begin{bmatrix} 0 \\ -\frac{1}{\Theta_y} \\ \kappa/\Theta_x + \Theta_y \end{bmatrix}. \tag{B.8}$$

where

$$D := \frac{\Theta_x - \Theta_y}{\Theta_x + \Theta_y}, \quad k := \frac{K}{\Theta_x + \Theta_y}. \tag{B.9}$$

From (B.5) and (B.6), B_S^B can be written as

$$B_S^B = (0, -\frac{\bar{p}_B \bar{r}_B}{\bar{f}_P}, \frac{k \bar{r}_B^2}{\bar{f}_P}). \tag{B.10}$$

Let R^{BC} be parametrized by the standard aeronautics Euler angle sequence with roll (ν), pitch (μ), and yaw (η) angles such that

$$R^{BC} = R_x(\nu) R_y(\mu) R_z(\eta). \tag{B.11}$$

Combining (9), (13) and (B.11) yields

$$\frac{\bar{p}_B}{\bar{\omega}} = -\sin \mu, \quad \frac{\bar{q}_B}{\bar{\omega}} = \cos \mu \sin \nu, \quad \frac{\bar{r}_B}{\bar{\omega}} = \cos \mu \cos \nu. \tag{B.12}$$

Since $\bar{q}_B = 0$ and $\bar{r}_B \neq 0$, it can be seen from (B.12) that $\sin \nu$ is equal to 0, which leads to $\nu = 0$.

With the second row of (14) the remaining degree of freedom η can be solved:

$$\cos(\nu) \sin(\mu) \sin(\eta) - \sin(\nu) \cos(\eta) = 0 \tag{B.13}$$

which yields

$$\eta = \arctan\left(\frac{\tan(\nu)}{\sin(\mu)}\right) = 0. \tag{B.14}$$

Therefore, the coordinate transformation from the C-frame to the B-frame is a rotation around the y-axis of the C-frame, that is,

$$R^{BC} = \begin{bmatrix} \cos \mu & 0 & -\sin \mu \\ 0 & 1 & 0 \\ \sin \mu & 0 & \cos \mu \end{bmatrix} \tag{B.15}$$

and $R^{BC} \bar{\omega}_{CE}^C = \bar{\omega}_{BE}^B$ leads to

$$\bar{p}_B = -\sin(\mu) \bar{\omega}, \quad \bar{r}_B = \cos(\mu) \bar{\omega}. \tag{B.16}$$

For brevity, let $\alpha = -\sin(\mu) > 0$ (since $\bar{p}_B > 0$) and $\beta = \cos(\mu) > 0$. Note that $\alpha^2 + \beta^2 = 1$.

Substituting (B.16) into A_S^B and B_S^B and applying coordinate transformation $A_S^C = R^{CB} A_S^B R^{BC}$ and $B_S^C = R^{CB} B_S^B$ yields

$$A_S^C = \begin{bmatrix} -2k\beta\alpha^2\bar{\omega} & (-\beta^2 - D\alpha^2)\bar{\omega} & 2k\beta^2\alpha\bar{\omega} \\ (\beta^2 - \alpha^2)\bar{\omega} & 0 & 2\beta\alpha\bar{\omega} \\ 2k\beta^2\alpha\bar{\omega} & (-\beta\alpha + D\beta\alpha)\bar{\omega} & -2k\beta^3\bar{\omega} \end{bmatrix} \tag{B.17}$$

and

$$B_S^C = \begin{bmatrix} -k\beta^2\alpha\bar{\omega}^2/\bar{f}_P & -\frac{\beta\alpha\bar{\omega}^2}{\bar{f}_P} & \frac{k\beta^3\bar{\omega}^2}{\bar{f}_P} \end{bmatrix}, \tag{B.18}$$

respectively.

Substituting $n_{P,z}^C = \beta$, (25), (B.17), and (B.18) into U_0 (A.8) and computing its determinant yields

$$\det(U_0) = -\frac{2k\beta^4\bar{\omega}^3}{m}(\beta^2 + \alpha^2)^2, \tag{B.19}$$

which is non-zero, meaning that $[-A_{11} \ B_1]$ has full rank.

For the eigenvalues $\pm\bar{\omega}i$, (A.15) becomes

$$U_i = \begin{bmatrix} 1 & \bar{\omega}i + 2k\beta\alpha^2\bar{\omega} & -(\beta^2 - \alpha^2)\bar{\omega} & -2k\beta^2\alpha\bar{\omega} \\ -i & (\beta^2 + D\alpha^2)\bar{\omega} & \bar{\omega}i & \beta\alpha\bar{\omega} - D\beta\alpha\bar{\omega} \\ 0 & -2k\beta^2\alpha\bar{\omega} & -2\beta\alpha\bar{\omega} & \bar{\omega}i + 2k\beta^3\bar{\omega} \\ 0 & -k\beta^2\alpha\bar{\omega}^2/\bar{f}_P & -\frac{\beta\alpha\bar{\omega}^2}{\bar{f}_P} & \frac{k\beta^3\bar{\omega}^2}{\bar{f}_P} \end{bmatrix}. \tag{B.20}$$

To compute its determinant, multiply its fourth row by $-2\bar{f}_P/\bar{\omega}$ and add to the third row and then compute its determinant yields

$$\det(U_i) = -i\frac{\beta\alpha\bar{\omega}^4}{\bar{f}_P}(-(\beta^2 + D\alpha^2) - 1). \tag{B.21}$$

Assume $\det(U_i) = 0$, then the following equation has to hold

$$\beta^2 + D\alpha^2 = 1, \tag{B.22}$$

simplifying which yields

$$\Theta_x - \Theta_y = \Theta_x + \Theta_y, \tag{B.23}$$

which is clearly a contradiction ($\Theta_y \neq 0$). Thus, $[\bar{\omega}iI - A_{11} \ B_1]$ has full rank.

For the eigenvalues of A_S^C , the matrix $[\lambda I - A_S^C \ B_S^C]$ has full rank for all λ is equivalent to the controllability of the matrix pair (A_S^C, B_S^C) (the PBH test), which is then equivalent to the full rankness of its associated controllability matrix

$$C = \begin{bmatrix} B_S^B & A_S^B B_S^B & (A_S^B)^2 B_S^B \end{bmatrix}. \tag{B.24}$$

Note that the matrix pair (A_S^B, B_S^B) with substitution from (B.16) is used instead, since coordinate transformation (which is the same as change of basis) does not affect the controllability of the linear system matrix pair, and it is easier to evaluate the controllability matrix C using the pair (A_S^B, B_S^B) .

Substituting (B.8) into C leads to

$$C = \frac{\beta\bar{\omega}^2}{\bar{f}_P} \begin{bmatrix} 0 & \beta\alpha\bar{\omega} & -k\beta^2\alpha\bar{\omega}^2 \\ -\alpha & k\beta\alpha\bar{\omega} & \alpha\bar{\omega}^2(\beta^2 - D\alpha^2 - 2k^2\beta^2) \\ k\beta & -(D\alpha^2 + 2k^2\beta^2)\bar{\omega} & k\beta\bar{\omega}^2(3Dr_2^2 + 4k^2\beta^2) \end{bmatrix}. \tag{B.25}$$

To compute its determinant, multiply the first and second column by $k\beta\bar{\omega}$ and add it to the second and third column, respectively, which

yields

$$C = \frac{\beta\bar{\omega}^2}{\bar{f}_P} \begin{bmatrix} 0 & \beta\alpha\bar{\omega} & 0 \\ -\alpha & 0 & \alpha\bar{\omega}^2(\beta^2 - D\alpha^2 - k^2\beta^2) \\ k\beta & -(D\alpha^2 + k^2\beta^2)\bar{\omega} & k\beta\bar{\omega}^2(2Dr_2^2 + 2k^2\beta^2) \end{bmatrix}. \quad (\text{B.26})$$

Again, multiply the second column by $2k\beta\bar{\omega}$ and add it to the third column

$$C = \frac{\beta\bar{\omega}^2}{\bar{f}_P} \begin{bmatrix} 0 & \beta\alpha\bar{\omega} & 2k\beta^2\alpha\bar{\omega}^2 \\ -\alpha & 0 & \alpha\bar{\omega}^2(\beta^2 - D\alpha^2 - k^2\beta^2) \\ k\beta & -(D\alpha^2 + k^2\beta^2)\bar{\omega} & 0 \end{bmatrix}. \quad (\text{B.27})$$

The determinant is then computed as

$$\det(C) = \frac{k\beta^5\alpha^2\bar{\omega}^9}{\bar{f}_P^3}(D\alpha^2 + \beta^2 + k^2\beta^2). \quad (\text{B.28})$$

Assume $\det(C) = 0$, by exploiting $\alpha^2 = 1 - \beta^2$,

$$D + \beta^2(k^2 - D + 1) = 0. \quad (\text{B.29})$$

Substituting the definition of D and k (B.9) back into the above equation yields

$$\beta^2 = \frac{\Theta_x^2 - \Theta_y^2}{-2\Theta_y^2 - 2\Theta_x\Theta_y - K^2}. \quad (\text{B.30})$$

If $\Theta_x^2 - \Theta_y^2 \geq 0$, clearly, the left hand side of (B.30) cannot be equal to its right hand side. Thus, the matrix C has full rank.

If $\Theta_x^2 - \Theta_y^2 < 0$, the eigenvalues of A_S^B are guaranteed to be stable. To see this, computing the characteristic polynomial of the matrix A_S^B (eigenvalues of a matrix stay invariant under coordinate transformation) leads to

$$\det(\lambda I - A) = \lambda^3 + \underbrace{2k\beta\bar{\omega}}_{a_1} \lambda^2 + \underbrace{(\beta^2\bar{\omega}^2 - \alpha^2\bar{\omega}^2 D)}_{a_2} \lambda + \underbrace{2k\beta^3}_{a_3} \bar{\omega}^3 = 0. \quad (\text{B.31})$$

According to the Routh–Hurwitz stability criterion, the poles of (B.31) have strictly negative parts if and only if the conditions $a_1 > 0$, $a_2 > 0$, $a_1 a_2 > a_3 > 0$ are fulfilled (Fact 11.17.2 [33]). This is clearly the case if $\Theta_x^2 - \Theta_y^2 < 0$ (i.e. $D < 0$) and recall that $k > 0$, $\beta > 0$, and $\bar{\omega} > 0$.

In conclusion, the system matrix pair (A_{11}, B_1) is at least stabilizable for this case.

B2. Controllability analysis for case 2

In this case (for assumptions see Section 3.2.3), we will show that the system is not stabilizable.

The Euler's equation simplifies to

$$\dot{p}_B = -\frac{J}{\Phi} p_B \|\omega_{BE}^B\| \quad (\text{B.32})$$

$$\dot{q}_B = -\frac{l}{\Theta} f_P - \frac{K}{\Theta} q_B \|\omega_{BE}^B\| + \frac{\Theta - \Phi}{\Theta} p_B r_B \quad (\text{B.33})$$

$$\dot{r}_B = \frac{\kappa}{\Theta} f_P - \frac{K}{\Theta} r_B \|\omega_{BE}^B\| + \frac{\Phi - \Theta}{\Theta} p_B q_B. \quad (\text{B.34})$$

Setting the left hand side of (B.32) to zero yields $\bar{p}_B = 0$.

Let the components of R^{BC} be

$$R^{BC} = [e_1 \quad e_2 \quad e_3] = \begin{bmatrix} r_1 & r_2 & r_3 \\ r_4 & r_5 & r_6 \\ r_7 & r_8 & r_9 \end{bmatrix}, \quad (\text{B.35})$$

where $e_i, i = 1, 2, 3$ denote the column vectors of R^{BC} , and $r_i, i = 1, \dots, 9$ denote the entries. Since R^{BC} is a coordinate transformation matrix, the column vectors satisfy the following properties:

$$e_1 \times e_2 = e_3 \quad (\text{B.36})$$

$$e_2 \times e_3 = e_1 \quad (\text{B.37})$$

$$e_3 \times e_1 = e_2. \quad (\text{B.38})$$

$R^{BC} \omega_{CE}^C = \bar{\omega}_{BE}^B$ can be written as

$$\bar{p}_B = \bar{\omega} r_3 = 0, \quad \bar{q}_B = \bar{\omega} r_6, \quad \bar{r}_B = \bar{\omega} r_9, \quad (\text{B.39})$$

which also leads to $r_3 = 0$.

Furthermore, by (14)

$$0 = n_{P,y}^C = (R^{CB} n_P^B)_2 = r_8, \quad (\text{B.40})$$

where $(R^{CB} n_P^B)_2$ denotes the second entry of $R^{CB} n_P^B$. Linearizing (B.32)–(B.34) around $(\bar{p}_B, \bar{q}_B, \bar{r}_B)$ yields

$$A_S^B = \begin{bmatrix} -j\bar{\omega} & 0 & 0 \\ -c\bar{r}_B & -k\bar{\omega} & 0 \\ c\bar{q}_B & 0 & -k\bar{\omega} \end{bmatrix} - \frac{k}{\bar{\omega}} \bar{\omega}_{BE}^B (\bar{\omega}_{BE}^B)^\top, \quad B_S^B = \begin{bmatrix} 0 & -l/\Theta & \frac{\kappa}{\Theta} \end{bmatrix}, \quad (\text{B.41})$$

where $j := \frac{J}{\Phi}$, $k := \frac{K}{\Theta}$ and $c := \frac{\Phi - \Theta}{\Theta}$.

Substituting (B.39) into A_S^B and applying coordinate transformation $A_S^C = R^{CB} A_S^B R^{BC}$ and some simplifications ((B.36)–(B.38), and (B.40)), it follows that

$$A_S^C = \begin{bmatrix} -k\bar{\omega} + cr_1 r_2 \bar{\omega} + r_1^2(k-j)\bar{\omega} & r_2^2 c \bar{\omega} + r_1 r_2(k-j)\bar{\omega} & r_2 r_3 c \bar{\omega} \\ -r_1^2 c \bar{\omega} + r_1 r_2(k-j)\bar{\omega} & -k\bar{\omega} - cr_1 r_2 \bar{\omega} + r_2^2(k-j)\bar{\omega} & r_1 r_3 c \bar{\omega} \\ 0 & 0 & -2k\bar{\omega} \end{bmatrix}. \quad (\text{B.42})$$

Substituting (B.39) into (B.33) and (B.34) and setting their left hand side to zero yields

$$-\frac{l}{\Theta} = \frac{1}{\bar{f}_P} k r_6 \bar{\omega}^2 \quad (\text{B.43})$$

$$\frac{\kappa}{\Theta} = \frac{1}{\bar{f}_P} k r_9 \bar{\omega}^2. \quad (\text{B.44})$$

Substituting (B.43) and (B.44) into B_S^B in (B.41) and simplifying $R^{CB} B_S^B$ yields

$$B_S^C = \begin{bmatrix} 0 & 0 & k\bar{\omega}^2/\bar{f}_P \end{bmatrix}. \quad (\text{B.45})$$

Substituting the (B.42) and (B.45) into the definition of U_i and computing its determinant leads to

$$\det(U_i) = 0. \quad (\text{B.46})$$

This implies that the modes associated with the eigenvalues $\pm \bar{\omega}i$ are not controllable, and the system is therefore not stabilizable.

B3. Controllability analysis for case 3

The simplified Euler equation (40) for this case (for assumptions see Section 3.2.3) has the form

$$\Theta_x \dot{p}_B = (\Theta_y - \Theta_z) q_B r_B - K_{d,xx} p_B \|\omega_{BE}^B\| \quad (\text{B.47})$$

$$\Theta_y \dot{q}_B = (\Theta_z - \Theta_x) p_B r_B - K_{d,yy} q_B \|\omega_{BE}^B\| \quad (\text{B.48})$$

$$\Theta_z \dot{r}_B = (\Theta_x - \Theta_y) p_B q_B - K_{d,zz} r_B \|\omega_{BE}^B\| + \kappa f_P. \quad (\text{B.49})$$

Linearizing the above three equations around the equilibrium $(0, 0, \sqrt{\kappa \bar{f}_P / K_{d,zz}})$ yields

$$A_S^B = \begin{bmatrix} -k_x \bar{\omega} & a\bar{r}_B & 0 \\ b\bar{r}_B & -k_y \bar{\omega} & 0 \\ 0 & 0 & -k_z \bar{\omega} \end{bmatrix}, \quad B_S^B = \begin{bmatrix} 0 \\ 0 \\ \kappa/\Theta_z \end{bmatrix} \quad (\text{B.50})$$

where $k_x := K_{d,xx}/\Theta_x$, $k_y := K_{d,yy}/\Theta_y$, $k_z := K_{d,zz}/\Theta_z$, $a := (\Theta_y - \Theta_z)/\Theta_x$, $b := (\Theta_z - \Theta_x)/\Theta_y$.

From (B.12) and (B.13) it can be solved that $\mu = \nu = \eta = 0$. Therefore, R^{BC} is a three dimensional identity matrix.

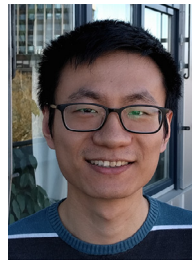
For the eigenvalue $\pm\omega i$, it is clear that $\det(U_i) = 0$. Thus the system for this case is not stabilizable.

Supplementary material

Supplementary material associated with this article can be found, in the online version, at doi:10.1016/j.mechatronics.2019.06.004.

References

- [1] Piccoli M. Passive stability and actuation of micro aerial vehicles. Ph.d. thesis; University of Pennsylvania; 2016.
- [2] Ulrich ER, Pines DJ, Humbert JS. From falling to flying: the path to powered flight of a robotic samara nano air vehicle. *Bioinspir Biomim* 2010;5(4):045009.
- [3] Houghton J, Hoburg W. Fly-by-wire control of a monocopter. Massachusetts Institute of Technology, Project Report; 2008.
- [4] Jameson S, Fregene K, Chang M, Allen N, Youngren H, Scroggins J. Lockheed martin's samurai nano air vehicle: challenges, research, and realization. In: 50th AIAA aerospace sciences meeting including the new horizons forum and aerospace exposition; 2012. p. 584.
- [5] Kellas A. The guided samara: design and development of a controllable single-bladed autorotating vehicle. Master's thesis; Massachusetts Institute of Technology; 2007.
- [6] Orsag M, Cesic J, Haus T, Bogdan S. Spincopter wing design and flight control. *J Intell Robot Syst* 2013;70(1–4):165–79.
- [7] Bakula M, Hockley C, Khatri R, Kirby C, Sammet C, Reinholtz C. A natural evolution in flight: the design and development of the samareye system, a method for searching closed quarter environments. In: First symp. on indoor flight issues; 2009. p. 1–12.
- [8] Piccoli M, Yim M. Piccolissimo: the smallest micro aerial vehicle. In: IEEE international conference on robotics and automation (ICRA); 2017. p. 3209–16.
- [9] Teoh ZE, Fuller SB, Chirarattananon P, Pérez-Arancia NO, Greenberg JD, Wood RJ. A hovering flapping-wing microrobot with altitude control and passive upright stability. In: IROS; 2012. p. 3209–16.
- [10] Breugel FV, Regan W, Lipson H. From insects to machines. *IEEE Robot Autom Mag* 2008;15(4).
- [11] McCutchen C. Flying machines, aeromodeler magazine; 1954. July.
- [12] Norberg RA. Autorotation, self-stability, and structure of single-winged fruits and seeds (samaras) with comparative remarks on animal flight. *Biol Rev* 1973;48(4):561–96.
- [13] Matic G, Topić M, Jankovec M. Mathematical model of a monocopter based on unsteady blade-element momentum theory. *J Aircr* 2015;52(6):1905–13.
- [14] Obradovic B, Ho G, Barto R, Fregene K, Sharp D. A multi-scale simulation methodology for the samurai monocopter μ av. In: AIAA modeling and simulation technologies conference; 2012. p. 5012.
- [15] Richards G. Christmas under control!. *Eng Technol* 2010;5(18):42–3.
- [16] Flower Flutterbye Fairy, Spin Masters; 2018. (Date last accessed 18-July-https://www.spinmaster.com/product_detail.php?pid=p10171).
- [17] De Wagter C, Tijmons S, Remes BD, de Croon GC. Autonomous flight of a 20-gram flapping wing mav with a 4-gram onboard stereo vision system. In: Robotics and automation (ICRA), 2014 IEEE international conference on, IEEE; 2014. p. 4982–7.
- [18] Ma KY, Chirarattananon P, Fuller SB, Wood RJ. Controlled flight of a biologically inspired, insect-scale robot. *Science* 2013;340(6132):603–7.
- [19] Keennon M, Klingebiel K, Won H. Development of the nano hummingbird: a tailless flapping wing micro air vehicle. In: 50th AIAA aerospace sciences meeting including the new horizons forum and aerospace exposition; 2012. p. 588.
- [20] Paulos J, Yim M. Flight performance of a swashplateless micro air vehicle. In: IEEE international conference on robotics and automation (ICRA); 2015. p. 5284–9.
- [21] b-IONIC Airfish, FESTO; 2018. (Date last accessed 16-July-https://www.festo.com/net/SupportPortal/Files/344798/b_IONIC_Airfish_en.pdf).
- [22] Drew DS, Lambert NO, Schindler CB, Pister KS. Toward controlled flight of the ionocraft: a flying microrobot using electrohydrodynamic thrust with onboard sensing and no moving parts. *IEEE Robot Autom Lett* 2018;3(4):2807–13.
- [23] Mueller MW, D'Andrea R. Stability and control of a quadcopter despite the complete loss of one, two, or three propellers. In: IEEE international conference on robotics and automation (ICRA), IEEE; 2014. p. 45–52.
- [24] Mueller MW, D'Andrea R. Relaxed hover solutions for multicopters: application to algorithmic redundancy and novel vehicles. *Int J Robot Res* 2016;35(8):873–89.
- [25] Du GX, Quan Q, Yang B, Cai KY. Controllability analysis for multirotor helicopter rotor degradation and failure. *J Guid Control Dyn* 2015;38(5):978–85.
- [26] Zhang W, Mueller MW, D'Andrea R. A controllable flying vehicle with a single moving part. In: IEEE international conference on robotics and automation (ICRA); 2016. p. 3275–81.
- [27] Martin P, Salaün E. The true role of accelerometer feedback in quadrotor control. In: IEEE international conference on robotics and automation (ICRA); 2010. p. 1623–9.
- [28] Pounds P, Mahony R, Hynes P, Roberts JM. Design of a four-rotor aerial robot. In: Proceedings of the 2002 Australasian Conference on Robotics and Automation (ACRA 2002), Australian robotics & automation association; 2002. p. 145–50.
- [29] Leishman GJ. Principles of helicopter aerodynamics with CD extra. Cambridge university press; 2006.
- [30] Etkin B, Reid LD. Dynamics of flight: stability and control, 3. Wiley New York; 1996.
- [31] Shuster MD. A survey of attitude representations. *Navigation* 1993;8(9):439–517.
- [32] Callier FM, Desoer CA. Linear system theory. Springer Science & Business Media; 2012.
- [33] Bernstein DS. Matrix mathematics: theory, facts, and formulas. Princeton reference, 2, editor. Princeton University Press; 2009.
- [34] Lupashin S, Hehn M, Mueller MW, Schoellig AP, Sherback M, Andrea RD. A platform for aerial robotics research and demonstration: the flying machine arena. *Mechatronics* 2014;24(1):41–54.
- [35] Bertsekas DP. Dynamic programming and optimal control, 1. Belmont, MA: Athena scientific; 2005.
- [36] Antsaklis PJ, Michel AN. Linear systems. Springer Science & Business Media; 2006.



Weixuan Zhang received his bachelor's degree in Mechanical Engineering from Karlsruhe Institute of Technology in 2013, and received the Grashof Prize for his outstanding bachelor studies. Subsequently, he started his master's study in Mechanical Engineering at ETH Zurich, with focus on control theory and robotics. He was awarded the Willi Studer prize 2016 for the best master degree in Mechanical Engineering. Since November 2015 he has been pursuing a doctorate at ETH Zurich.



Mark W. Mueller joined the mechanical engineering department at UC Berkeley in September 2016, where he leads the High Performance Robotics Laboratory (HiPeRLab), working primarily on aerial robotics. He completed his Ph.D. studies, advised by Prof. Raffaello D'Andrea, at the Institute for Dynamic Systems and Control at the ETH Zurich at the end of 2015. He received a bachelors degree from the University of Pretoria, and a masters from the ETH Zurich in 2011, both in Mechanical Engineering.



Raffaello D'Andrea received the B.Sc. degree in Engineering Science from the University of Toronto in 1991, and the M.S. and Ph.D. degrees in Electrical Engineering from the California Institute of Technology in 1992 and 1997. He was an assistant, and then an associate, professor at Cornell University from 1997 to 2007. While on leave from Cornell, from 2003 to 2007, he co-founded Kiva Systems (now Amazon Robotics), where he led the systems architecture, robot design, robot navigation and coordination, and control algorithms development. He is currently professor of Dynamic Systems and Control at ETH Zurich, and chairman of the board at Verity Studios AG.